Tribology and Materials
Vol. 2, No. 1, 2023, pp. 32-37

ISSN 2812-9717
https://doi.org/10.46793/tribomat.2023.001

Three-dimensional modelling of tensile behaviour for standard aluminium specimens

Zaigham Saeed TOOR

Department of Materials Science and Engineering, Institute of Space Technology, Islamabad, Pakistan
zaighamtoor93@gmail.com

Keywords

aluminium alloy
material testing
finite element analysis
stress magnification

History

Received: 27-01-2023
Revised: 21-02-2023
Accepted: 23-02-2023

Abstract

The effect of specimen width and incorporation of a circular hole on the tensile behaviour of commercially available aluminium alloy AA 1100 was studied using finite element analysis (FEA) for convergence with the already published experimental work of other researchers. Static structural analysis was conducted to simulate tensile loading of Japanese industrial standard (JIS) specimen JIS Z 2201 No. 13B and No. 5 until the point of the ultimate tensile strength (UTS) was reached. A strain rate of 0.25 mm/s was used for both the neat specimen and the one bearing a circular hole of 8 mm in diameter at the centre of the specimen. The numerical results exhibited a good agreement with the experimental work by comparison of the percentage elongation for numerical and experimental data. The normal stresses calculated using analytical and numerical approaches also reflected a good convergence. For neat specimens of JIS Z 2201 No. 13B and No. 5, a 100 % increase in specimen width enhanced the load required to reach UTS by 100 %, while elongation was increased by 30 %. On the other hand, for specimens of JIS Z 2201 No. 13B and No. 5, bearing an 8 mm circular hole reduced the load required to reach UTS by 300 %, while elongation was only increased by 25 %. The 200 % decrease in load required to reach UTS and 57 % reduction in elongation was observed by incorporating an 8 mm circular hole in the neat specimens.

1. Introduction

Aluminium and its alloys have tremendous applications in almost all of the available industries, namely aerospace, automobiles, food and beverages, construction, composites and even the defence industry is not new to this class of materials [1,2]. Their wide range of properties, namely good formability, high specific strength, good corrosion resistance and cost-effectiveness make them a potential candidate of interest for various designers, manufacturers and industrialists [3,4].

Aluminium alloy AA 1100 is one of the purest commercially available wrought alloys which has various cold worked designations available to increase mechanical strength, namely H18, H16 and H14. Due to its good workability, thermal conductivity, corrosion resistance and strength, it has various applications in rivets, sheet metal and cooking utensils [5,6].

Finite element analysis (FEA) is an effective computational approach to solving various engineering problems by modelling a situation according to the applied boundary conditions and then obtaining a solution using different mathematical models. ANSYS is commercially available software that is frequently used to simulate such problems to obtain a numerical solution [7-11].

Stress magnification and stress concentration are commonly defined as an increase in the stress of a specimen at the same applied load due to surface or subsurface circular holes or flaws that act as points of stress risers which result in premature failure of the material as compared to the predicted load and stress [12-17].

This article has used FEA to acquire a numerical solution to the results presented by Sulamet-Ariobimo et al. [5] to study the effect of specimen width and circular hole presence on the tensile behaviour of the specimens.

2. Methodology

2.1 Material properties

Sulamet-Ariobimo et al. [5] have discussed mechanical testing of commercially available AA 1100 using JIS Z 2201 No. 13B and No. 5 standard flat sheet non-proportional type specimens, providing a desired failure region under tensile loading. The nominal chemical composition and mechanical properties of the alloy with the designation H14 are mentioned in Tables 1 and 2, respectively. Dimensions of the specimens are shown in Figures 1 and 2, respectively.

Table 1. Nominal chemical composition of AA 1100

Element	Cu	Mn	Zn	Si+Fe	Other	Al
wt. %	0.05–0.20	0.05	0.1	0.95	0.15	99.3

Table 2. Mechanical properties of AA 1100 [5]

Property	Value
Density, g/cm^3	2.71
Modulus of elasticity, GPa	69
Poisson's ratio	0.33
Yield strength, MPa	105
Ultimate tensile strength, MPa	124

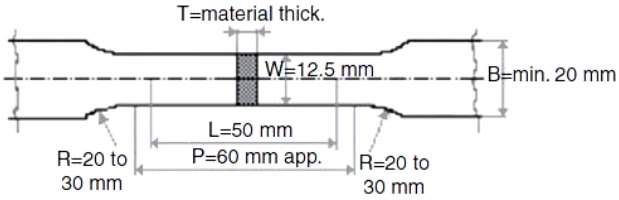

Figure 1. Dimensions of tensile specimen JIS Z 2201 No. 13B; reprinted from Sulamet-Ariobimo et al. [5], licensed under CC BY-NC-ND 4.0

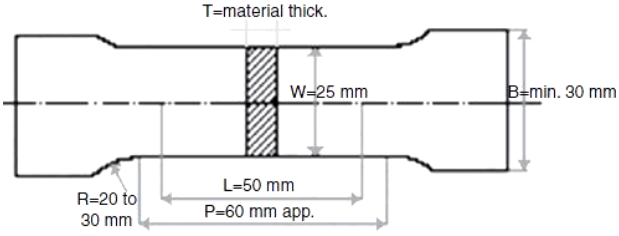

Figure 2. Dimensions of tensile specimen JIS Z 2201 No. 5; reprinted from Sulamet-Ariobimo et al. [5], licensed under CC BY-NC-ND 4.0

2.2 Numerical modelling

A static structural module was used to model the tensile behaviour of both specimens until ultimate tensile strength was reached. Boundary conditions were set according to specifications mentioned by Sulamet-Ariobimo et al. [5] as shown in Table 3. A circular hole of 8 mm in diameter was also incorporated into the specimens to compare the effect of the stress riser under the same boundary conditions.

Table 3. Boundary conditions applied [5]

Condition	Value
Fixed support end	*x*-axis
Strain rate (displacement)	0.25 mm/s (*x*-axis)
Specimen thickness	2 mm

2.3 Meshing

Mesh sensitivity analysis was done for model calibration using stress and deformation as the output parameters. After iterative element size optimisation, when less than 5 % change in the output parameters was observed irrespective of the element size, the meshing criteria were finalised for all specimens as shown in Table 4 [7,8,18,19]. Figure 3 represents the meshing and boundary conditions of the tensile specimen.

Table 4. Meshing criteria

Specimen	Type	Mesh type (SOLID186 and SOLID187)	Nodes	Elements
JIS Z 2201 No. 13B	neat	brick	749	88
	8 mm circular hole	triangular	76,865	3725
JIS Z 2201 No. 5	neat	brick	948	115
	8 mm circular hole	triangular	10,188	4882

2.4 Analytical solution

The theoretical and numerical normal stresses at a fixed load of 150 N were also compared as per the procedure mentioned in [12]. The maximum

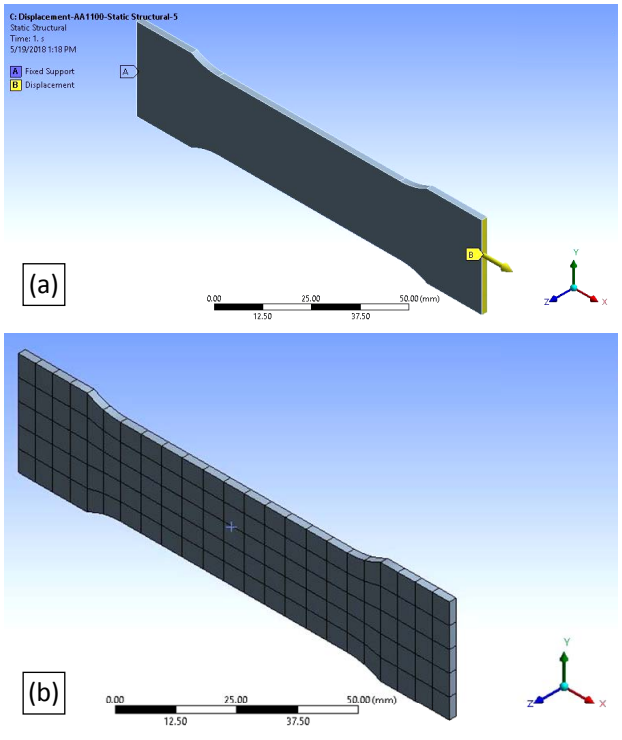

Figure 3. Tensile specimen: (a) boundary conditions and (b) meshing conditions

average normal stress through the cross-section of the specimens was calculated analytically by dividing it against the applied force. The same was evaluated numerically using finite element analysis (FEA). A quantitative comparison was made using graphical visualisations for validation of the model.

3. Results and discussion

In order to validate the finite element model, the percentage elongation reported by Sulamet-Ariobimo et al. [5] was compared with the numerical analysis results. The experimental results showed a 32 % increase in elongation while the numerical results showed an increase of 30 % in elongation. This indicated that the variation between numerical and experimental results was less than 7 %, indicating good convergence and validation of the model for further parametric analysis.

Figures 4 to 7 show the stress distribution for each specimen under the above-mentioned meshing and boundary conditions. It can be seen that for both neat specimens, irrespective of the specimen width, uniform stress distribution along the gauge length was observed. However, for the circular hole specimens, the stress was majorly concentrated along the circular region of the circular hole since it acted as a stress riser.

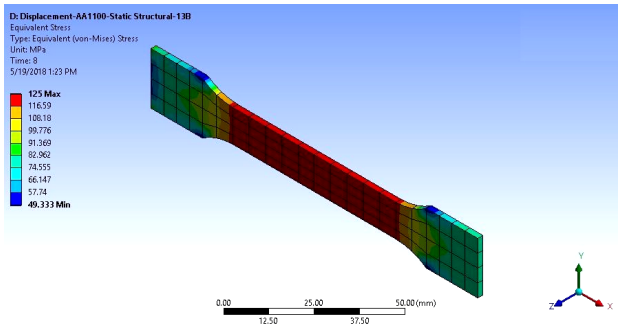

Figure 4. Stress distribution for neat tensile specimen JIS Z 2201 No. 13B

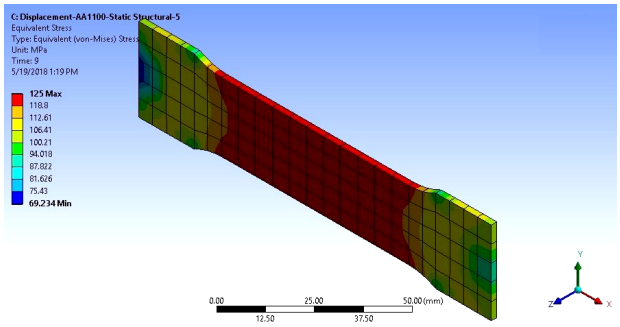

Figure 5. Stress distribution for neat tensile specimen JIS Z 2201 No. 5

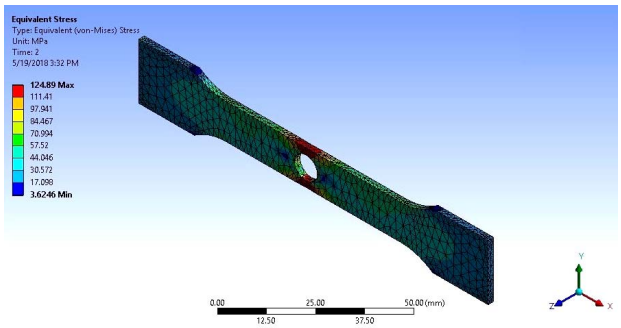

Figure 6. Stress distribution for tensile specimen JIS Z 2201 No. 13B with an 8 mm circular hole in the centre

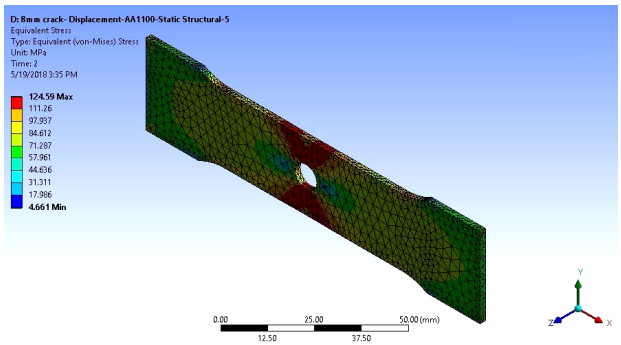

Figure 7. Stress distribution for tensile specimen JIS Z 2201 No. 5 with an 8 mm circular hole in the centre

Figures 8 and 9 show the load-deflection curves for the neat and circular hole specimens, respectively. It can be seen that as the specimen width has increased, the load required to reach UTS and the total deflection have also increased

for both, the neat and the circular hole specimen. By comparing the neat specimens with their circular hole counterparts, it was observed that both, the load required to reach UTS and the total deflection or elongation decreased for the circular hole specimens.

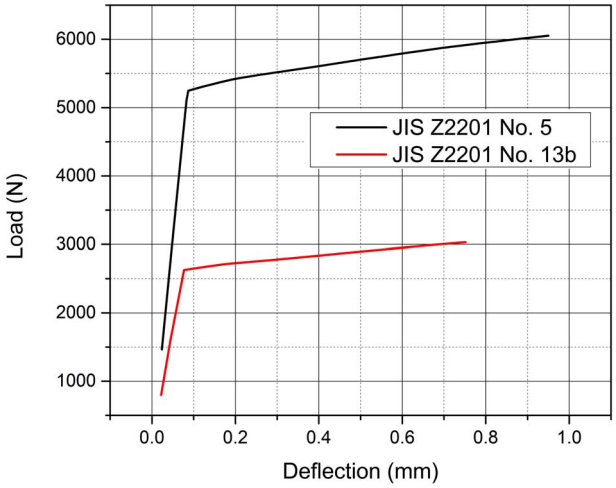

Figure 8. Load-deflection diagram for neat tensile specimen JIS Z 2201 No. 13B and No. 5

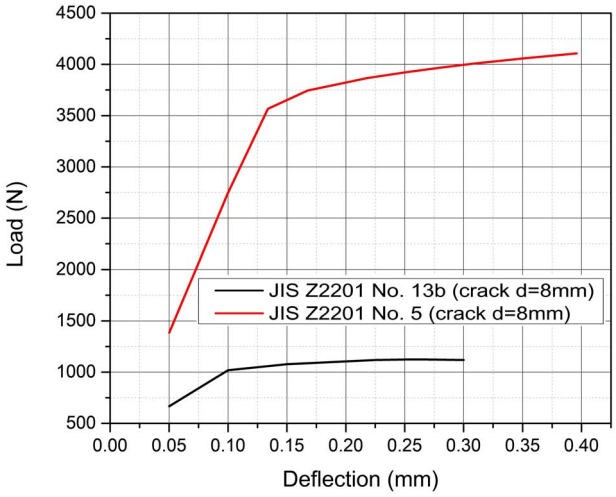

Figure 9. Load-deflection diagram for tensile specimen JIS Z 2201 No. 13B and No. 5 with an 8 mm circular hole in the centre

Table 5 shows for different specimen widths the results of load at UTS and percentage elongation at UTS for both, the neat and circular hole specimens. The results discussed by Sulamet-Ariobimo et al. [5] showed a 32 % increase in elongation while the numerical results showed an increase of 30 % in elongation. The numerical results exhibited a good agreement with the experimental work. For neat specimens JIS Z 2201 No. 13B and No. 5, a 100 % increase in specimen width, enhanced the load required to reach UTS by 100 %, while elongation was increased by 30 %. On the other hand, for specimens JIS Z 2201 No. 13B and No. 5, bearing an 8 mm circular hole, a 100 % increase in specimen width reduced the load required to reach UTS by 300 %, while elongation was only increased by 25 %. A 200 % decrease in load required to reach UTS and a 57 % reduction in elongation was observed by incorporating an 8 mm circular hole in the neat specimens.

Table 5. Results of simulation

Specimen	Type	Width, mm	Load, N	Elongation, %
JIS Z 2201 No. 13B	neat	12.5	3000	1.4
	8 mm circular hole	12.5	1000	0.6
JIS Z 2201 No. 5	neat	25	6000	2
	8 mm circular hole	25	4000	0.8

Figure 10 shows the comparison between theoretically calculated analytical normal stresses on both types of specimens with their corresponding numerical counterparts. The comparison was made for the maximum average normal stresses through the cross-section of the specimen thickness. For the analytical calculations, the corresponding cross-sectional area was reduced by increasing the diameter of the circular hole, while for the numerical models, each model was developed separately by changing the diameter of the circular hole and then updating the final specimen before meshing.

It was observed that irrespective of the specimen type, the normal stress in the structure increased with the subsequent increase in the diameter of the circular hole. Moreover, specimen JIS Z 2201 No. 13B reflected an exponential increase in the normal stress, while specimen JIS Z 2201 No. 5 showed a linear increase in the normal stress against the same corresponding diameter of a circular hole. This can be attributed to their respective geometrical properties, i.e. the former specimen has a smaller cross-sectional area than the latter specimen due to which, at the same load, the respective stress is larger in the specimen with the least cross-sectional area. A good convergence between the theoretical and numerical results was observed with a variation of less than 5 %.

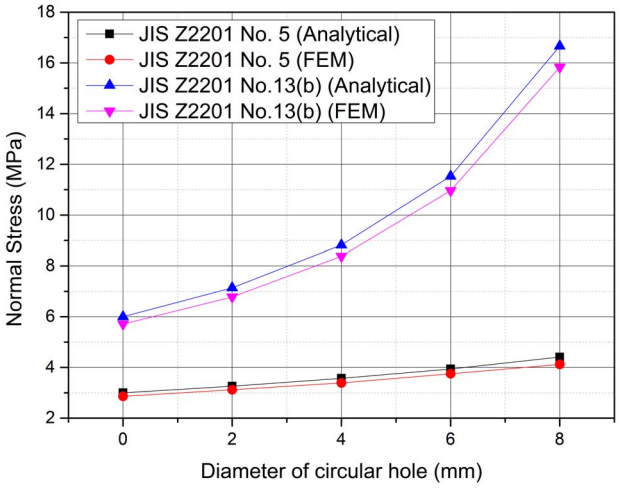

Figure 10. Analytical versus FEM results for normal stress against the diameter of a circular hole

4. Conclusion

A finite element model for standardised tensile specimens has been successfully calibrated and validated by using appropriate meshing density, followed by a convincing comparison with already published experimental results. The effect of the circular hole on the stress generated in the respective specimens has been analysed numerically, which indicates an exponential and linear increase in the normal stress, depending upon the size of the circular hole and the geometric properties of the specimen. A good convergence between the analytical, numerical and experimental results has been observed with an overall variation in the results being less than 5 %. Since tensile testing is a core area of material testing, especially in the automotive and aerospace industries, this calibrated and validated model can be augmented with experimental apparatuses for the universal testing machines (UTM) available in different engineering universities, as well as, the industries using the standardised tensile specimens. The same can be used for parametric analysis, material comparison, structural integrity and risk assessment studies.

Acknowledgement

The author would like to express his gratitude to the Smart Composites Laboratory (SComp-Lab), Department of Materials Science and Engineering (MS&E), Institute of Space Technology (IST) for providing the computing facility for this research.

References

[1] A. Vencl, A. Rac, I. Bobić, Tribological behaviour of Al-based MMCs and their application in automotive industry, Tribology in Industry, Vol. 26, No. 3-4, 2004, pp. 31-38.

[2] J. Hirsch, Aluminium alloys for automotive application, Materials Science Forum, Vol. 242, 1997, pp. 33-50, DOI: 10.4028/www.scientific.net/MSF.242.33

[3] A.H. Musfirah, A.G. Jaharah, Magnesium and aluminum alloys in automotive industry, Journal of Applied Sciences Research, Vol. 8, No. 10, 2012, pp. 4865-4875.

[4] M. Wenzelburger, M. Silber, R. Gadow, Manufacturing of light metal matrix composites by combined thermal spray and semisolid forming process – Summary of the current state of technology, Key Engineering Materials, Vol. 425, 2010, pp. 217-244, DOI: 10.4028/www.scientific.net/KEM.425.217

[5] R.D. Sulamet-Ariobimo, J.W. Soedarsono, T. Sukarnoto, A. Rustandi, Y. Mujalis, D. Prayitno, Tensile properties analysis of AA1100 aluminium and SS400 steel using different JIS tensile standard specimen, Journal of Applied Research and Technology, Vol. 14, No. 2, 2016, pp. 148-153, DOI: 10.1016/j.jart.2016.03.006

[6] E.A. Starke, J.T. Staley, Application of modern aluminum alloys to aircraft, Progress in Aerospace Sciences, Vol. 32, No. 2-3, 1996, pp. 131-172, DOI: 10.1016/0376-0421(95)00004-6

[7] S. Du, Z. Zhu, C. Liu, T. Zhang, M.M. Hossain, H.-J. Sue, Experimental observation and finite element method modeling on scratch-induced delamination of multilayer polymeric structures, Polymer Engineering and Science, Vol. 61, No. 6, 2021, pp. 1742-1754, DOI: 10.1002/pen.25697

[8] S. Du, M. Mullins, M. Hamdi, H.-J. Sue, Quantitative modeling of scratch behavior of amorphous polymers at elevated temperatures, Polymer, Vol. 197, 2020, Paper 122504, DOI: 10.1016/j.polymer.2020.122504

[9] J. Grün, S. Feldmeth, F. Bauer, The sealing mechanism of radial lip seals: A numerical study of the tangential distortion of the sealing edge, Tribology and Materials, Vol. 1, No. 1, 2022, pp. 1-10, DOI: 10.46793/tribomat.2022.001

[10] M.K. Bhuarya, M.S. Rajput, A. Gupta, Finite element simulation of impact on metal plate, Procedia Engineering, Vol. 173, 2017, pp. 259-263, DOI: 10.1016/j.proeng.2016.12.009

[11] Z.S. Toor, Effect of drill on mechanical and modal characteristics of aluminum sheet, Journal of Space Technology, Vol. 11, 2021, pp. 14-19.

[12] Z.S. Toor, Finite element method for numerical stress analysis of aluminum plate, Journal of Space Technology, Vol. 10, 2020, pp. 1-6.

[13] Z.S. Toor, Parametric optimization using finite element analysis based virtual framework, Journal of Space Technology, Vol. 12, 2022, pp. 1-5.
[14] Z.S. Toor, M.M. Zafar, Corrosion degradation of aluminium alloys using a computational framework, Tribology and Materials, Vol. 1, No. 4, 2022, pp. 150-156, DOI: 10.46793/tribomat.2022.019
[15] D. Ngo, A.C. Scordelis, Finite element analysis of reinforced concrete beams, Journal of American Concrete Institute, Vol. 64, No. 3, 1967, pp. 152-163, DOI: 10.14359/7551
[16] W. Kastner, E. Röhrich, W. Schmitt, R. Steinbuch, Critical crack sizes in ductile piping, International Journal of Pressure Vessels and Piping, Vol. 9, No. 3, 1981, pp. 197-219, DOI: 10.1016/0308-0161(81)90002-8
[17] Z.S. Toor, Influence of crack morphology and its distribution on stress magnification of AA2024-T3, Journal of Space Technology, Vol. 10, 2020, pp. 50-57.
[18] G. Molero, S. Du, M. Mamak, M. Agerton, M.M. Hossain, H.-J. Sue, Experimental and numerical determination of adhesive strength in semi-rigid multi-layer polymeric systems, Polymer Testing, Vol. 75, 2019, pp. 85-92, DOI: 10.1016/j.polymertesting.2019.01.012
[19] S. Du, M. Hamdi, H.-J. Sue, Experimental and FEM analysis of mar behavior on amorphous polymers, Wear, Vol. 444-445, 2020, Paper 203155, DOI: 10.1016/j.wear.2019.203155